ISSN 0023-1584, Kinetics and Catalysis, 2018, Vol. 59, No. 6, pp. 828–836. © Pleiades Publishing, Ltd., 2018.
Original Russian Text © P.A. Chernavskii, O.L. Eliseev, R.V. Kazantsev, G.V. Pankina, N.E. Strokova, A.L. Lapidus, 2018, published in Kinetika i Kataliz, 2018, Vol. 59, No. 6, pp. 795–803.

Effect of Topochemical Processes in the Synthesis of FeK/C Catalysts on Their Activity and Selectivity in the Fischer–Tropsch Synthesis

P. A. Chernavskii[a], *, O. L. Eliseev[b], R. V. Kazantsev[b], G. V. Pankina[a], N. E. Strokova[a], and A. L. Lapidus[c]

[a] *Department of Chemistry, Moscow State University, Moscow, 119991 Russia*
[b] *Zelinsky Institute of Organic Chemistry, Russian Academy of Sciences, Moscow, 119991 Russia*
[c] *Gubkin State University of Oil and Gas, Moscow, 119991 Russia*
**e-mail: chern5@inbox.ru*

Received March 5, 2018

Abstract—Iron-containing catalysts promoted with potassium supported on a carbon carrier were prepared by changing the sequence of the introduction of components (iron and potassium) into the carrier (activated carbon) using an impregnation method. After calcination, the catalysts contained hematite and magnetite; in this case, the particle sizes of iron oxides depended on the sequence of the introduction of a potassium promoter. A minimum particle size was observed upon the subsequent introduction of initially potassium from nitrate and then iron. The activation of all of the catalysts in a flow of CO/H_2 resulted in the formation of Hägg carbide (Fe_5C_2). It was shown that the catalyst with the smallest carbide particle size was the most active in the hydrogenation of CO.

Keywords: iron oxide nanoparticles, promotion, catalyst, activated carbon, carbides, Fischer–Tropsch synthesis

DOI: 10.1134/S0023158418060022

The Fischer–Tropsch (FT) synthesis is a key step in the production of liquid hydrocarbons from coal, natural gas, or biomass [1, 2]. Moreover, the direct conversion of synthesis gas ($CO + H_2$) into light C_2–C_4 olefins without intermediate stages, the so-called Fischer–Tropsch-to-Olefins (FTO) process, is a promising alternative method for the production of high-value chemicals [3, 4]. Iron-containing catalysts for the FT synthesis are more preferable than cobalt catalysts, which are more active, because they are less expensive and exhibit higher selectivity for the formation of olefins. The results of studies [5, 6] have shown that supported iron-containing catalysts have undeniable advantages over unsupported catalysts. In turn, the use of carbon carriers has good prospects because of their weak interaction with a catalytically active phase. It was assumed [7, 8] that the distribution of the active component of a catalyst and a promoter affects the process selectivity of the FT synthesis. It was reported [9, 10] that potassium facilitates the carbonization of iron and increases the probability of chain growth.

The simplest way to prepare a promoted catalyst is the co-impregnation of the support with an aqueous solution of the salts of an active component and a promoter. However, it is not obvious that this is the best method for producing an active catalyst. In a number of works [11–14], the influence of the sequence of introducing components into a catalyst on its activity and selectivity was studied. The method used for introducing promoters and the type of iron compounds play a decisive role in the development and production of highly active, selective, and stable iron-based composite systems. Duan et al. [11] obtained a catalyst, which was a composite of carbon nanotubes and iron and potassium oxides, by a redox reaction between carbon nanotubes and K_2FeO_4 with the subsequent heat treatment. The study of samples prepared by impregnation with the subsequent heat treatment showed that the new composite catalyst had relatively high activity, greater selectivity for hydrocarbons and short olefins, and better stability, and it increased the probability of chain growth.

For the conversion of synthesis gas into ethanol, Wang et al. [12] modified a rhodium catalyst supported on silicon dioxide with various transition metal oxides. They found that iron oxide is an effective promoter of ethanol formation. It turned out that the way of introducing FeO_x significantly affects the conversion and selectivity. The catalyst prepared by the impregnation of a FeO_x–SiO_2 composite, which was synthesized previously by a sol–gel method, with an

aqueous solution of $Rh(NO_3)_3$ provided better activity in the synthesis of ethanol than that of the samples prepared by combined impregnation. Ledford et al. [13] prepared $CoLa/Al_2O_3$ catalysts by the following two methods: impregnation with a salt of La and then with a salt of Co (Co/La) and impregnation with a salt of Co and then with a salt of La (La/Co). The La–Co interaction was absent from the La/Co samples.

Gnanamani and coworkers [14] studied the effect of the order of phosphorus and cobalt addition to silica in the course of the synthesis of Fischer–Tropsch catalysts. They found that the preliminary application of phosphorus increased the dispersity of cobalt and, thereby, facilitated an increase in the activity of the sample in the FT synthesis and its selectivity for heavy hydrocarbons. On the contrary, the introduction of phosphorus after cobalt had a negative effect on the conversion of CO and on selectivity for C_{5+} hydrocarbons.

The main purpose of this work was to study the effect of the sequence of introduction of components on the activity and selectivity of a FeK/C catalyst. The catalysts were prepared by the following three methods: the co-impregnation of an activated carbon carrier with the solutions of iron and potassium nitrates, the sequential impregnation with the solutions of $Fe(NO_3)_3$ and then KNO_3, and the sequential impregnation with the reverse order of introduction of the components.

EXPERIMENTAL

Catalyst Preparation

The catalyst synthesis procedure included the following sequence of operations: the preparation of the nitrate solutions of KNO_3 (analytical grade) and $Fe(NO_3)_3 \cdot 9H_2O$ (analytical grade); the impregnation of activated carbon (AC) (VEB Laborchemie Apolda; specific surface area, 819 m^2/g) with one of the solutions; drying in a rotary evaporator at 80°C; and calcination at 450°C for 3 h in a flow of nitrogen. Then, the procedure was repeated with the second component, iron nitrate or potassium nitrate. Thus, catalysts with different sequences of introducing the potassium promoter were obtained. The concentration of nitrate solutions was 50%, and the calculated concentrations of iron and potassium in the catalysts were 15 and 2 wt %, respectively. In addition, a catalyst was prepared by co-impregnating the support with a mixture of iron and potassium nitrates in the same percentage. Henceforth, the catalysts are referred to as K/Fe/C, Fe/K/C, and (FeK)/C, where the application sequence should be read from right to left. The catalyst samples containing only iron or only potassium and a catalyst prepared by co-impregnation were also synthesized; in this case, the catalysts were only dried rather than calcined. This series of samples was intended for studying by differential thermal analysis (DTA) and magnetometry.

The elemental composition of the surfaces of the resulting catalysts was determined by energy-dispersive X-ray spectroscopy (EDS) using a JSM-6490LV scanning electron microscope (JEOL, Japan). The bulk composition of the catalysts was analyzed by an inductively coupled plasma (ICP) method using an ICP-5000 instrument (Focused Photonics, South Korea).

Differential Thermal Analysis

The test sample was heated from 40 to 600°C at a rate of 10 K/min in an inert atmosphere (in a flow of argon at 80 mL/min) in a Netzsch STA 449 C Jupiter thermal analyzer (Netzsch, Germany). In the course of heating, effluent gases were supplied to an Aeolos QMS 403C quadrupole mass spectrometer (Netzsch, Germany) for scanning ionized fragments over an m/z range from 10 to 50.

Magnetometry

The kinetic studies of the samples were conducted on a vibrating-coil magnetometer in the in situ mode. The test samples with a weight of 10 mg were placed in the measuring cell of a vibrating-coil magnetometer [15], which was a flow microreactor with a volume of 0.3 cm^3. The test sample was tightly fixed between two porous quartz membranes. For all of the initial catalysts and catalysts after activation in synthesis gas, the dependences of magnetization on the magnetic field strength were obtained and the saturation magnetization, residual magnetization, and coercive force were measured. The gas flow rate was 10 mL/min in all of the experiments. The gases were preliminarily passed through a column with γ-Al_2O_3 heated to 300°C for the removal of iron carbonyls. In a nonisothermal experiment, the sample was heated to a specified temperature in a flow of CO (or synthesis gas). The heating to a specified temperature was performed at a rate of 10 K/min; in this case, changes in the magnetization were continuously measured with a frequency of 1 Hz. After reaching the required temperature, the sample was cooled at a rate of 10 K/min in a CO/H_2 gas flow and the temperature dependence of magnetization was measured. In an isothermal experiment, the test sample was heated to a specified temperature in a flow of argon; then, the flow of argon was replaced by a flow of CO (or synthesis gas) and changes in the magnetization with time were also measured thereafter. An IR detector was arranged at the reactor outlet to measure continuously the rate of CO_2 formation. In some cases, when it was necessary to more accurately

determine the Curie temperature, the sample after reaching room temperature was repeatedly heated in a flow of argon and the change in magnetization was measured. As a result, we obtained thermomagnetic functions, which allowed us to determine the Curie temperature of the resulting phase with a sufficiently high accuracy; this temperature was found as the intersection point of a tangent to an extremum point of the thermomagnetic curve with the x-axis. Bends in the thermomagnetic curve indicated the occurrence of several magnetic phases. In this case, the type of a magnetic phase according to the Curie temperature can be determined based on the position of a bend in the curve. An analysis of thermomagnetic curves in the presence of two magnetic phases also makes it possible to determine the quantitative composition of magnetic phases in the test sample [16].

Transmission Electron Microscopy

The microstructure of the samples was studied by transmission electron microscopy (TEM) using a LEO912 AB OMEGA transmission electron microscope (Zeiss, Germany) with an image resolution of 0.2–0.34 nm at an accelerating voltage of 60–120 V. The test sample as a suspension in ethanol or distilled water was applied to a carbon film arranged on copper microgauze. The particle size distribution was obtained by a visual analysis of the micrographs. The distributions found were described by the logarithmically normal distribution

$$f(d) = \frac{1}{d\sigma\sqrt{2\pi}}\exp\left[-\frac{(\ln d - \mu)^2}{2\sigma^2}\right],$$

and the average crystallite size was determined from the formula

$$\bar{d} = \exp\left[\mu + \frac{\sigma^2}{2}\right].$$

Catalytic Tests

The productivity of the catalysts in the Fischer–Tropsch synthesis was tested in a steel fixed-bed downflow reactor (internal diameter, 16 mm). A catalyst portion of 200 mg was mixed with 1 cm^3 of quartz sand to prevent the formation of hot spots during the synthesis of hydrocarbons, and this mixture was loaded into the isothermal zone of the reactor. The samples were activated at atmospheric pressure in a flow of synthesis gas ($CO : H_2 = 1 : 2$) at 400°C for 2 h; thereafter, they were tested in the synthesis of hydrocarbon at $T = 240$°C and $P = 20$ bar. The initial gas composition was $CO : H_2$: Ar = 0.32 : 0.64: 0.04, and the specific gas flow rate was 16 L g_{Cat}^{-1} h^{-1}. The catalytic activity was evaluated after 20 h of operation upon reaching a pseudo-stationary regime. The composition of the gaseous products (C_1–C_4 hydrocarbons and CO_2) was determined on an LKhM-80 gas chromatograph (Russia) with columns (1 × 3 mm) packed with molecular sieves 5A and Porapak Q; helium was a carrier gas, and a katharometer was used as a detector. The C_{5+} liquid hydrocarbons were collected in a receiver at ambient temperature and analyzed on a Biochrom-1 chromatograph (Russia) using a quartz capillary column (50 m × 0.25 mm), an OB-101 stationary phase, nitrogen as a carrier gas, and a flame-ionization detector. Selectivity for the formation of C_{5+} products was calculated by difference between the total balance weight of carbon and the amount of C_1–C_4 and CO_2 gases.

RESULTS AND DISCUSSION

An analysis of the results of DTA (Figs. 1a and 1b) revealed a significant endothermic effect in a temperature range from 106 to 120°C for all of the test catalysts, which was accompanied by the release of water and a noticeable weight loss of the samples. At temperatures of about 210–215°C, a strong exothermic effect was noted with the concomitant formation of CO_2 and NO (Fig. 1b). At $T > 300$°C, the rate of weight loss decreased; the release of CO_2 and NO was strongly slowed down (Fig. 1b), and the removal of water completely stopped. The total weight loss of the samples upon calcination at 450°C was ~30%. The formation of CO_2 and NO indicated the oxidation of the surface of a carbon matrix with the possible formation of carboxyl groups. The thermal decomposition of iron nitrate is a complex multistage process [17] with the concomitant sequential removal of water and nitric acid molecules. At an elevated temperature, the hydroxide oxide $Fe_4O_4(OH)_4$ was formed, which was then converted into hematite Fe_2O_3. In the case of potassium nitrate supported onto activated charcoal, the release of CO_2 and NO was observed at temperatures of 170–200 and 295°C in the course of calcination in a flow of Ar. Note that the main weight loss and an exothermic effect were also observed at these temperatures. A noticeable exothermic effect at $T =$ 120°C, accompanied by a weight loss and the formation of CO^2 and NO, was detected only in the presence of iron nitrate in the system. The sample weight loss, the exothermic effect, and the two peaks of the release of CO_2 and NO strongly correlated with each other. This circumstance allowed us to assume that the process of the oxidation of an activated carbon carrier with the formation of CO_2 occurred in two temperature ranges and coincided with the appearance of NO.

According to the results shown in Fig. 1, the main part of the processes of thermolysis was complete at $T \le 300$°C. However, an increase in magnetization due to the formation of magnetite Fe_3O_4 could be observed in the course of thermolysis in a magnetometer cell [18]. Thus, the partial reduction of hematite to magnetite occurred in the course of thermolysis of iron nitrate on a carbon substrate along with nitrate decomposition.

The elemental composition of the surface of the catalysts differed significantly from the average bulk composition (Table 1), mainly in terms of the iron content. The difference between the surface concentration of iron and the average bulk concentration was 13 wt % for all of the catalysts except for Fe/K/C (11.5 wt %). In our opinion, this difference was due to the partial hydrolytic decomposition of iron nitrate in the mouths of the pores of carrier granules. In contrast, the potassium concentration in the catalysts containing the promoter was slightly lower on the surface than in the bulk. From the data given in Table 1, it follows that the greatest amount of magnetite was formed on calcination in the catalysts where iron was first supported onto the carrier (63 and 81% of theoretically possible for Fe/C and K/Fe/C, respectively). In the samples of Fe/K/C and (FeK)/C, the fractions of magnetite were much lower: 48 and 31% of the calculated values, respectively. The appearance of magnetite upon calcination indicates the partial reduction of Fe^{3+} to Fe^{2+}. In this case, only the carbon of the carrier, which is in direct contact with iron oxides, can be a reducing agent. The preliminary application of potassium markedly decreased the amount of magnetite. We believe that this was due to the inhibitory effect of potassium on the process of hematite reduction to magnetite [19].

An analysis of the results of transmission electron microscopy showed a regular decrease in the average particle size of iron oxides in the order Fe/C > K/Fe/C > (FeK)/C > Fe/K/C, which was accompanied by a decrease in the dispersion of the distribution. Figure 2 shows the histograms of the particle size distributions of iron oxide. In our opinion, the decrease in the particle size of iron oxide (mainly Fe_3O_4) was due to a decrease in the rate of hematite reduction in the presence of potassium. Another reason could be the interaction of the carrier surface with KNO_3 supported during high-temperature processing. It is likely that the decomposition of the nitrate ion occurred simultaneously with the surface oxidation of activated carbon with the formation of oxygen-containing groups (hydroxyl, carboxyl, etc.) on the surface. The adsorption of Fe^{3+} ions on these groups was more intense than on the pure carrier; this led to the appearance of a larger number of the crystallite growth centers for iron oxides and, correspondingly, to a decrease in their size than that in the case of Fe/C and K/Fe/C samples.

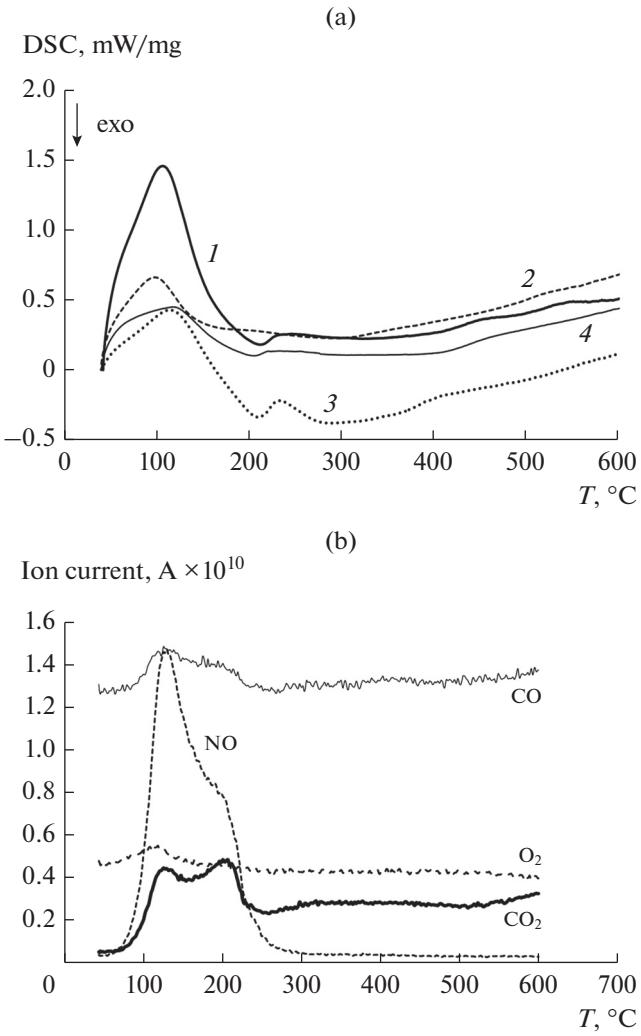

Fig. 1. (a) Results of the differential thermal analysis of the catalysts: (*1*) $Fe(NO_3)_3 \cdot 9H_2O$/C, (*2*) KNO_3/C, (*3*) $(Fe(NO_3)_3 \cdot 9H_2O + KNO_3)$/C, and (*4*) $(Fe(NO_3)_3 9H_2O$/K/C. (b) The mass spectrum of gases released in the course of the DTA of the Fe/C catalyst.

Figure 3 shows hysteresis loops for the test catalysts. The presence of a coercive force should be noted, which is indicative of the occurrence of nonsuperparamagnetic particles or the agglomerates of superparamagnetic particles in the catalysts.

Activation of Catalysts on Heating in a Flow of Synthesis Gas

Figure 4 shows changes in the magnetization with temperature in the course of catalyst activation in a flow of synthesis gas under the conditions of linear heating. Its initial decrease up to 280–290°C was due

Table 1. Surface composition and magnetite content of the initial catalysts

Catalyst	Surface composition, wt %		Bulk composition, wt %		Volume, wt % Fe_3O_4*	Calculated concentration of Fe_3O_4**
	Fe	K	Fe	K		
Fe/C	29	–	16	0.05	14	22
K/Fe/C	26	1.0	12.5	1.06	14	17.2
Fe/K/C	20	0.7	8.5	0.9	5.6	11.7
(FeK)/C	27	1.7	14	1.85	5.9	19

* Calculated from the measurements of saturation magnetization.
** The amount of magnetite calculated on the condition that iron entirely occurred as magnetite. A dash indicates the absence of the element.

to the temperature dependence of the magnetization of magnetite, which was initially present in the catalysts. However, in the course of heating, a nonmonotonic change in the magnetization was observed due to competition between the two processes: the decrease of magnetization with temperature and the occurrence of chemical reactions accompanied by the formation of new phases. The following two temperature ranges in which the magnetization increased can be recognized: the 300–350 and 420–550°C ranges for the K/Fe/C and Fe/C catalysts and 270–370 and 370–570°C for the (FeK)/C and Fe/K/C catalysts, respectively. Thus, all of the samples exhibited similar behaviors: an increase in the magnetization with the subsequent decrease to a minimum value and then a growth again. A further increase in the temperature led to a drop in the magnetization to zero, which corresponded to the Curie temperature of one of the magnetic phases. The cooling of the catalyst to room temperature in a flow of synthesis gas made it possible to obtain thermomagnetic curves from which the Curie temperatures were found for the magnetic phases formed as a result of activation. The Curie temperature was determined as the as the intersection point of a tangent to an extremum point of the thermomagnetic curve with the x-axis.

As follows from Fig. 5, all of the catalysts exhibited the formation of Hägg carbide (Fe_5C_2) with a characteristic Curie temperature of 250 ± 5°C. Additional experiments were carried out to explain the reason for the nonmonotonic change in the magnetization during the activation of the samples. Heating was interrupted at the extremum points of the curves, and the catalyst was cooled to room temperature. The subsequent analysis of the thermomagnetic curves obtained upon cooling showed that the first maximum corresponded to a magnetite phase, which was apparently formed upon the partial reduction of hematite. Upon cooling from a minimum point, the magnetization at room temperature was very small. Presumably, the minimum point corresponded to the formation of wustite, which is an antiferromagnetic material. The next maximum indicated the presence of magnetite and Hägg carbide χ-Fe_5C_2. Upon cooling from a temperature corresponding to zero magnetization, the formation of the χ-Fe_5C_2 carbide with a Curie temperature of 250°C was observed in all of the catalysts. Thus, the temperature dependence of the magnetization observed during activation can be described by the following sequence of chemical reactions:

$$3Fe_2O_3 + CO = 2Fe_3O_4 + CO_2,$$
$$3Fe_2O_3 + H_2 = 2Fe_3O_4 + H_2O,$$
$$Fe_3O_4 + CO = 3FeO + CO_2,$$
$$Fe_3O_4 + H_2 = 3FeO + H_2O,$$
$$5FeO + 9CO = Fe_5C_2 + 7CO_2,$$
$$FeO + H_2 = Fe + H_2O,$$
$$5Fe + 4CO = Fe_5C_2 + 2CO_2.$$

The amount of carbide formed can be determined from the saturation magnetization. Table 2 shows the carbide content (wt %) in the samples measured and calculated under the condition of the complete conversion of iron into carbide after the activation process. The calculation was based on the amount of iron according to ICP analysis data. However, if we used the results of the analysis of surface composition, we obtained other ratios between the calculated and experimentally determined carbide concentrations because magnetic measurements gave average bulk values (Table 3). Table 3 summarizes the average particle sizes of iron oxides obtained from TEM data and the calculated specific surface area of carbide particles. This surface area was calculated based on the assumption that the size of carbide particles was exactly the same as that of iron oxides, and the concentration of iron in the catalyst corresponded to its concentration on the surface. The calculated specific surface area of carbide particles noticeably increased markedly in the Fe/K/C and (FeK)/C catalysts, that is, in the cases when potassium was supported onto the carbon carrier preliminarily or simultaneously with iron nitrate.

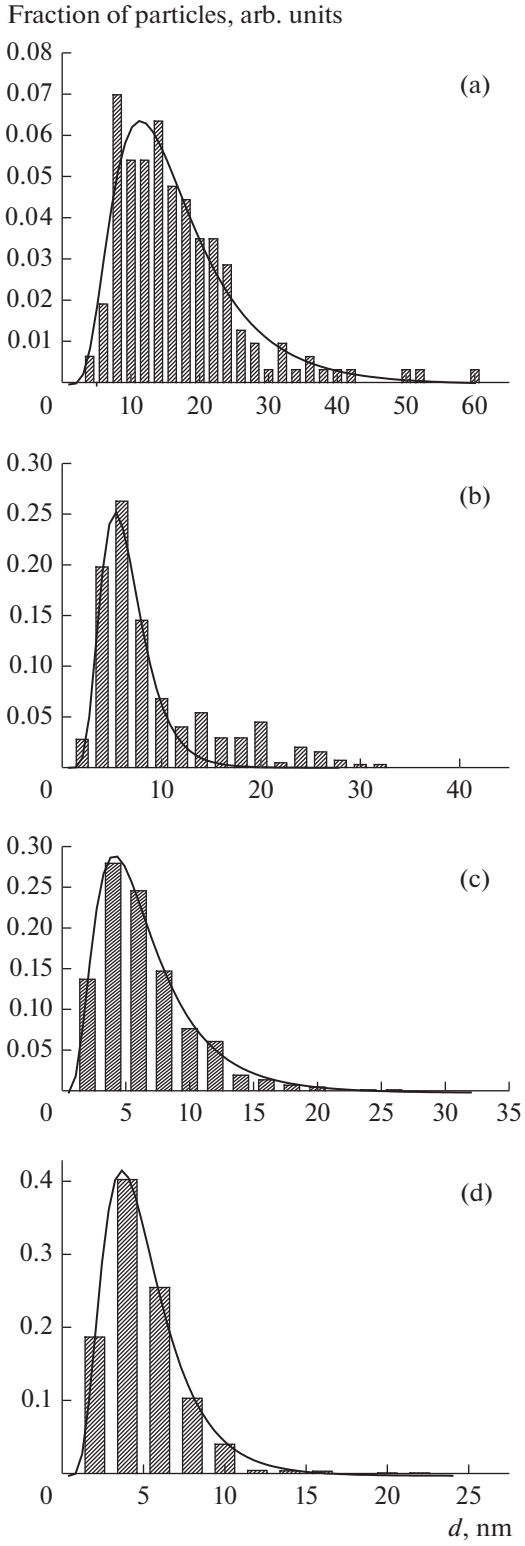

Fig. 2. Histograms of the particle size distributions based on the transmission electron microscopy data: (a) Fe/C, (b) K/Fe/C, (c) (FeK)/C, and (d) Fe/K/C.

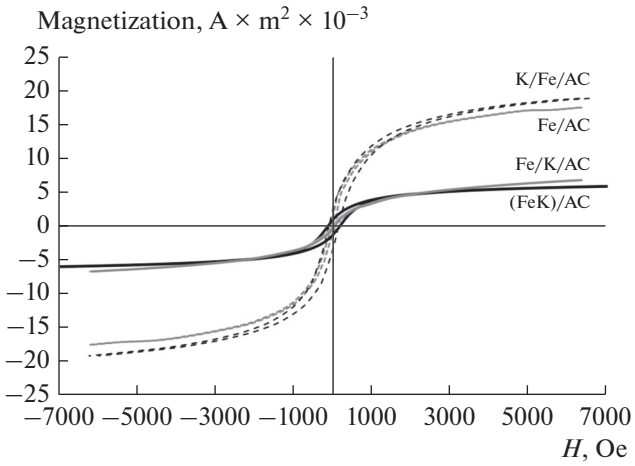

Fig. 3. Dependence of the magnetization on the field intensity for the initial catalysts.

Tables 4 and 5 summarize the results of the catalytic tests. The conversion of carbon monoxide and selectivity for CO_2 significantly increased with the addition of potassium to the catalyst. Apparently, this was due to both the intensification of the water gas shift reaction to form CO_2 and the promoting effect of the alkaline additive on the formation of higher hydrocarbons. In contrast, selectivity for methane changed only slightly upon the addition of the promoter.

The most interesting result was the effect of the sequence of introducing active components (iron and potassium) into the catalysts on their specific activity and selectivity. Thus, among the promoted catalysts, the activity (expressed as the amount of CO converted on 1 mol of Fe per second) was maximal for the Fe/K/C catalyst or minimal for K/Fe/C, whereas the (FeK)/C sample prepared by joint impregnation had an intermediate value of this characteristic. All of the three samples were more active than the Fe/C free of the promoter (Fig. 6).

A comparison of data on the activity with the particle size distributions of magnetite in the samples showed that a sharper distribution with a small average particle size of magnetite was characteristic of the most active catalysts. In contrast, samples with a wide distribution and an increased average particle size were less active. It is reasonable to assume that the particle size of the Fe_5C_2 carbide, which was formed at the stage of catalyst activation as an active phase in the synthesis of hydrocarbons, correlates with the size of the initial magnetite particles. Thus, an increase in the specific active surface area regularly leads to an increase in the activity of the catalyst.

The catalysts obtained by sequential impregnation exhibited minimal selectivity for C_{5+}, whereas the jointly impregnated sample showed almost the same selectivity as that of the nonpromoted Fe/C. The addition of potassium led to an increase in the fraction of light olefins, especially, on the catalysts obtained by

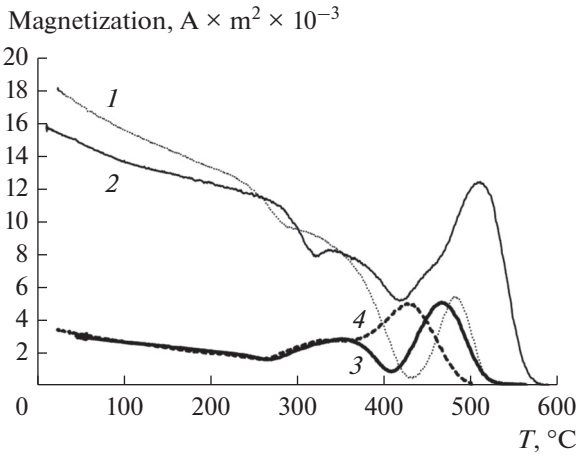

Fig. 4. Dependence of the magnetization on temperature in the course of catalyst activation in synthesis gas: (*1*) K/Fe/C, (*2*) Fe/C, (*3*) (FeK)/C, and (*4*) Fe/K/C.

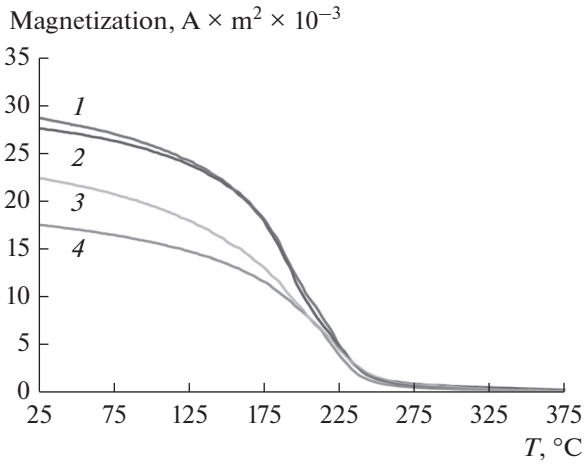

Fig. 5. Dependence of the magnetization of the catalysts on temperature after their activation in the synthesis gas: (*1*) K/Fe/C, (*2*) Fe/C, (*3*) (FeK)/C, and (*4*) Fe/K/C.

sequential impregnation. On the contrary, the olefin content of heavier products was almost independent of the addition of potassium. The molecular weight distribution of synthesized hydrocarbons corresponded to the Anderson–Schulz–Flory (ASF) formula [20]. A significant increase in the distribution parameter α was observed upon the addition of potassium. Therefore, heavier products were formed on the promoted catalysts (Table 5).

The aqueous phase formed in the synthesis was analyzed for the content of organic products. Only C_1–C_4 alcohols were detected in it, and their amount varied greatly depending on the catalyst preparation method. The catalysts promoted with potassium afforded a smaller amount of alcohols than that obtained on Fe/C (Table 4). Alcohols almost exclusively contained linear isomers, and only trace

Table 2. ron concentrations in the samples according to ICP data and the amount of carbide in the catalysts after treatment in CO/H_2, as determined experimentally and calculated from the ICP data

Catalyst	Fe, wt % (ICP)	Fe_5C_2, wt % theoretical* (ICP)	Fe_5C_2, wt % experimental**	Degree of Fe conversion into Fe_5C_2
Fe/C	16	17	14	0.82
Kn/Fe/C	12.5	14	12.5	0.89
Fe/Kn/C	8.5	9.2	9.2	1
(FeKn)/C	14	15	15	1

* Calculated based on the assumption of the complete conversion of Fe into Fe_5C_2 carbide.
** The amount of Fe_5C_2 carbide experimentally determined from the saturation magnetization data.

Table 3. The iron content of the near-surface layer of catalysts, the amount of carbide in the bulk of the samples, and the sizes and specific surface areas of the carbide particles

Catalyst	Fe, wt % surface*	Fe_5C_2, wt % surface theoretical**	Fe_5C_2, wt % experimental	*d*, nm***	S_{sp}, m^2/g****
Fe/C	29	31.5	14	16	2.3
Kn/Fe/C	26	28	12.5	6	5.6
Fe/Kn/C	21	23	9.2	4	6.8
(FeKn)/C	28	30.4	15	6	6

* Surface concentration of Fe based on the scanning electron microscopy data.
** The amount of Fe_5C_2 carbide on the surface was calculated assuming the complete conversion of surface Fe into the Fe_5C_2 carbide.
*** Average particle size of iron oxides according to the TEM data.
**** Calculated specific surface area of carbide particles on the catalyst surface (**).

Table 4. Characteristics of the catalytic activity of samples in the Fischer–Tropsch synthesis*

Catalyst	Conversion of CO, %	Selectivity for carbon, mol %		
		hydrocarbons	alcohols	CO_2
Fe/C	32.2	89.2	5.7	5.1
Kn/Fe/C	62.0	84.5	1.8	13.7
Fe/Kn/C	87.2	78.9	2.3	18.8
(FeKn)/C	86.1	77	4.0	19.0

* Reaction conditions: $T = 240°C$, $P = 20$ bar, $CO : H_2 : Ar = 0.32 : 0.64 : 0.04$, and specific gas flow rate of 16 L g_{Cat}^{-1} h^{-1}.

Table 5. Composition of the Fischer–Tropsch synthesis products *

Catalyst	Distribution of hydrocarbons, mol % in terms of carbon					O/(O + P), % **		ASF distribution parameter	
	CH_4	C_2	C_3	C_4	C_{5+}	C_2–C_4	C_{5+}	α_p ***	α_a ****
Fe/C	9.3	5.2	3.2	4.6	77.8	36.6	16.2	0.787	0.284
Kn/Fe/C	9.2	5.9	8.7	4.2	72.1	50.0	16.2	0.852	0.273
Fe/Kn/C	9.7	5.8	9.6	4.6	70.3	51.2	13.0	0.830	0.380
(FeKn)/C	7.9	4.4	5.4	4.7	77.5	37.3	15.4	0.836	0.347

* Conditions: $T = 240°C$, $P = 20$ bar, $CO : H_2 : Ar = 0.32 : 0.64 : 0.04$, and specific gas flow rate of 16 L g_{Cat}^{-1} h^{-1}.
** The proportion of olefins in hydrocarbon fractions.
*** The Anderson–Schulz–Flory distribution parameter for C_5–C_{25} *n*-alkanes.
**** The Anderson–Schulz–Flory distribution parameter for C_1–C_4 alcohols.

amounts of isopropanol were determined. The relative amounts of alcohols corresponded to the ASF distribution, but their values of the parameter α were much lower than those of paraffins (Table 5). This may be explained by different structures of the surface intermediates involved in the growth of the hydrocarbon chains of paraffins and alcohols.

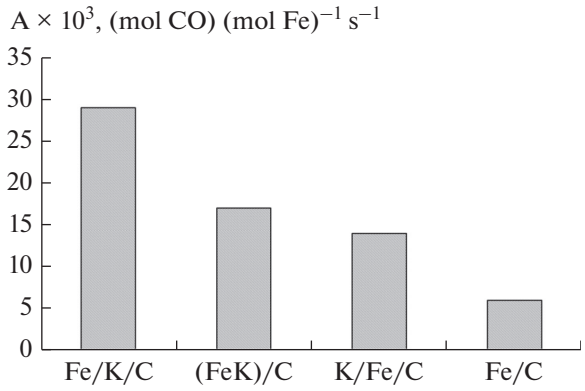

Fig. 6. Dependence of the specific activity on the type of catalysts.

CONCLUSIONS

We found that the sequence of the supporting of active components onto potassium-promoted iron catalysts affected a number of their physicochemical and catalytic properties. The preliminary application of potassium to a carbon carrier led to a significant decrease in the size of the magnetite particles formed upon the subsequent application of iron nitrate and calcination. A difference between the iron content of the surface of carrier granules and the average bulk concentration of iron was found. We assumed that this effect was due to the hydrolytic thermolysis of iron nitrate in the surface layer of activated carbon granules in the course of the catalyst synthesis. Potassium inhibited the reduction of hematite to magnetite on catalyst activation in CO/H_2, which led to the formation of smaller magnetite particles. The formation of Hägg carbide (Fe_5C_2) occurred in the course of catalyst activation in an atmosphere of synthesis gas. We found that the catalyst with a minimum carbide particle size and a maximum carbide concentration on the surface of granules had the greatest activity in the Fischer–Tropsch synthesis.

ACKNOWLEDGMENTS

This work was supported by the Russian Foundation for Basic Research (grant no. 16-03-00215-a).

REFERENCES

1. Huber, G.W., Iborra, S., and Corma, A., *Chem. Rev.*, 2006, vol. 106, p. 4044.
2. van Steen, E. and Claeys M., *Chem. Eng. Technol.*, 2008, vol. 31, p. 655.
3. Torres Galvis, H.M. and de Jong K.P., *ACS Catal.*, 2013, vol. 3, p. 2130.
4. Snel, R., *Catal. Rev. Sci. Eng.*, 1987, vol. 29, p. 361.
5. Torres Galvis, H.M., Bitter, J.H., Khare, C.B., Ruitenbeek, M., Dugulan, A.I., and de Jong, K.P., *Science*, 2012, vol. 335, p. 835.
6. Yang, Z.Q., Pan, X.L., Wang, J.H., and Bao, X.H., *Catal. Today*, 2012, vol. 186, p. 121.
7. Bezemer, G.L., Radstake, P.B., Falke, U., Oosterbeek, H., Kuipers, H.P.C.E., van Vandillen, A.J., and de Jong, K.P., *J. Catal.*, 2006, vol. 237, p. 152.
8. Morales, F., Grandjean, D., de Groot, F.M.F., Stephan, O., and Weckhuysen, B.M., *Phys. Chem. Chem. Phys.*, 2005, vol. 7, p. 568.
9. Ribeiro, M.C., Jacobs, G., Davis, B.H., Cronauer, D.C., Kropf, A.J., and Marshall, C.L., *J. Phys. Chem. C*, 2010, vol. 114, p. 7895.
10. Luo, M.S., O'Brien, R.J., Bao, S.Q., and Davis, B.H., *Appl. Catal., A*, 2003, vol. 239, p. 111.
11. Duan, X., Wang, D., Qian, G., Walmsley, J.C., Holmen, A., Chen, D., and Zhou, X., *J. Energy Chem.*, 2016, vol. 25, p. 311.
12. Wang, J., Zhang, Q., and Wang, Y., *Catal. Today*, 2011, vol. 171, p. 257.
13. Ledford, J.S., Houalla, M., Proctor, A., Hercules, D.M., and Petrakis, L., *J. Phys. Chem.*, 1989, vol. 93, p. 6770.
14. Kumaran, G.M., Jacobs, G., Graham, U.M., Pendyala, V.R.R., Martinelli, M., MacLennan, A., Hu, Y., and Davis, B.H., *Appl. Catal., A*, 2017, vol. 538, p. 190.
15. Chernavskii, P.A., Lunin, B.S., Pankina, G.V., Zakharyan, R.A., and Perov, N.S., *Instrum. Exp. Tech.*, 2014, vol. 57, no. 1, p. 78.
16. Selwood, P.W., *Magnetochemistry*, Interscience Publishing Company: N.-Y., 194, p. 287 p.
17. Melnikov, P., Nascimento, V.A., Arkhangelsky, I.V., Consolo, Z., and de Oliveira, L.C.S., *J. Therm. Anal. Calorim.*, 2014, vol. 115, p. 145.
18. Chernavskii, P.A., Kazak, V.O., Pankina, G.V., Strokova, N.E., and Perfil'ev, Yu.D., *Kinet. Katal.*, 2018, vol. 59, no. 2, p. 251.
19. Kazak, V.O., Pankina, G.V., Chernavskii, P.A., and Lunin, V.V., *Russ. J. Phys. Chem. A*, 2017, vol. 91, no. 5, p. 822.
20. Friedel, R.A. and Anderson, R.B., *J. Am. Chem. Soc.*, 1950, vol. 72, p. 1212.

Translated by V. Makhlyarchuk

SPELL: 1. OK